Communications in Computational Chemistry
Commun. Comput. Chem., Vol. 7, No. 4, 361–371
doi: 10.4208/cicc.2025.192.01
Regular Article

Adsorption of Some Pteridine-Based Compounds on Fe (110) Surface and Potential for Corrosion Inhibition: Quantum Computations Molecular Dynamics Simulations

Ekemini Ituen[1,2*], Godstime Chuwkudike[1,2], Ubong Essien[3], Bright Daniel[4], Prince Micheal[5], Adebola Oyeniran[6], Muhammad Oshafu[7], Aduanya David[8] and Udoinyang Inyang[9]

[1]*Computational Materials Science Group, TETFUND Centre of Excellence in Computational Intelligence, University of Uyo, Uyo 52003, Nigeria;*

[2]*Department of Chemistry, Faculty of Physical Sciences, University of Uyo, Uyo, Nigeria;*

[3]*Department of Animal and Environmental Biology, University of Uyo, Uyo, Nigeria;*

[4]*Department of Chemistry, College of Arts and Sciences, University of Tennessee, Knoxville, USA;*

[5]*Department of Pure and Industrial Chemistry, University of Port Harcourt, Nigeria;*

[6]*Department of Chemistry, University of Lagos, Lagos, Nigeria;*

[7]*Department of Physics, Federal University of Lafia, Nasarawa State, Nigeria;*

[8]*Department of Mechanical Engineering, Michael Okpara University of Agriculture, Umudike, Nigeria;*

[9]*Department of Data Science, Faculty of Computing, University of Uyo, Uyo, Nigeria.*

[*] Corresponding authors: ekeminiituen@uniuyo.edu.ng

Received on 11 July 2025; Accepted on 22 August 2025

Abstract: The adsorption of organic molecules onto steel surfaces has been a key strategy in the selection of materials for mitigation of corrosion in various aggressive media. Computational chemistry offers valuable insight into the electronic interactions that govern this process. In this study, five pteridine-based compounds, namely, isoxanthopterin, leucopterin,

lumazine, pterin and xanthopterin, were assessed for their adsorption behaviour and corrosion inhibition potential on Fe(110) surface using density functional theory (DFT) and molecular dynamics (MD) simulations. Geometry optimization, frontier molecular orbital analysis, and quantum reactivity descriptors were computed using the B3LYP/DNP level of theory via the Dmol³ module in BIOVIA Material Studio. Fukui indices and Mulliken charge distributions were analyzed to predict adsorption sites. Additionally, adsorption energies and molecular configurations on the Fe(110) surface were examined using the Forcite and Adsorption Locator tools. Results showed that all the studied compounds exhibit planar geometries favorable for surface interaction, with isoxanthopterin and xanthopterin demonstrating the strongest adsorption energies. Key adsorption sites were localized around nitrogen and oxygen heteroatoms. The compounds are predicted to form stable interactions with the iron surface through both physisorption and chemisorption, indicating excellent potential for use as green corrosion inhibitors.

Key words: adsorption energy, corrosion inhibition, DFT, Fukui function, HOMO and LUMO, molecular dynamics simulation.

1. Introduction

The interface between the surface of metallic or alloy materials and organic compounds presents a rich and interesting phenonemon, particularly in corrosion science. This phenomenon is termed adsorption, and it is the central process underlying corrosion inhibition, whereby organic molecules interact with the alloy or metal surface to form a protective film that minimizes degradation [1]. The protective film forms due to either physical (electrostatic) interactions or chemical bonding between electron-rich sites on the inhibitor and the active sites on the surface [2].

Corrosion, especially in steel used across the construction, petrochemical, and marine sectors, contributes to significant economic loss and structural failure globally. Traditional methods for corrosion prevention often involve the use of corrosion inhibitors, which are mainly organic molecules with heteroatoms such as N, O, or S, that can adsorb onto the steel surface and prevent corrosive species from reaching the metal surface [3-5]. Despite the wide array of organic molecules investigated for this purpose, the corrosion inhibition potential of pteridine-based compounds remains relatively underexplored.

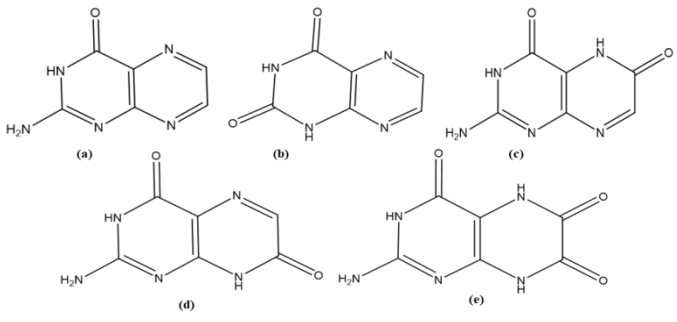

Figure 1. Molecular structures of (a) pterin (b) lumazine (c) xanthopterin (d) isoxanthopterin and (e) leucopterin.

Pteridine is a bicyclic nitrogen-containing heterocyclic compound, made specifically up of a fused pyrimidine and pyrazine ring. It is characterized by two nitrogen atoms at positions 1 and 4 in the pyrimidine ring (ring A) and two nitrogen atoms at positions 1 and 3 in the pyrazine ring (ring B). Pteridine and its derivatives are nitrogen-rich heterocycles structurally related to purines and flavins. They are known for their stable planar configurations and multiple functional groups capable of engaging in surface interactions. Compounds such as isoxanthopterin, leucopterin, lumazine, pterin and xanthopterin contain multiple electron-donating sites, making them strong candidates for corrosion inhibition. In addition, a careful look at the chemical structures of the molecules (Figure 1) would clearly reveal some variations in the functionalities attached to the pteridine moeities, which could give rise to interesting comparative and quantitative structure-function behaviour and mechanism of adsorption.

Some studies have reported various nitrogen-containing heterocycles such as imidazoles, triazoles and pyridines as corrosion inhibitors due to their high electron density and ability to coordinate with metal surfaces [6-8]. Despite their unique fused ring structure containing two nitrogen atoms in a diazine configuration, very little or nothing is known about the adsorption behaviour of these compounds, especially on iron based surfaces. The molecular structure, as it appears, may enhance surface adsorption and corrosion inhibition. To the best of our knowledge, few (if any) studies have employed pteridine derivatives specifically for corrosion inhibition on iron surfaces, especially using DFT-based predictive analysis. This study thus pioneers the evaluation of pteridine derivatives as potential eco-friendly inhibitors with promising electronic and adsorption properties.

The mechanism of interaction of organic molecules on surfaces and resultant corrosion inhibition is a complex one [9], hence, experimental studies alone are often insufficient in decoding the molecular-level mechanisms. In addition, experiments and laboratory procedures for cossorion monitoring, tests and assessments are associated with considerable cost, time, energy and safety limitations. Computational chemistry, particularly density functional theory (DFT) and molecular dynamics (MD) simulations, has emerged as a robust predictive tool that complements experimental approaches [10-12]. These methods provide insights

into molecular reactivity, electron distribution, adsorption energetics, and surface affinities [13].

In this work, density functional theory (DFT) calculations and molecular dynamics (MD) simulations were employed to investigate the adsorption behaviour of five pteridine-based inhibitors on the Fe(110) surface. The work focused on understanding molecular reactivity and predicting the potential active sites through frontier orbital analysis, Fukui functions, and adsorption energy calculations, with a view to evaluating their potential application as corrosion inhibitors. The five pteridine derivatives were selected based on their structural diversity, especially variation in electron-donating and -withdrawing substituents (e.g., $–NH_2$, =O). These substituents are known to influence adsorption behaviour on metal surfaces. Moreover, their precursors are readily available and can be synthesized through well-established routes. Prior theoretical assessments in other biological systems have suggested their stability and interactive potential, making them strong candidates for corrosion inhibition analysis [14, 15]. The findings could contribute toward the design of efficient, environmentally benign corrosion control agents for various real-life deployment.

2. Computational method

2.1 Geometry optimization

All molecular structures of the studied pteridine derivatives were constructed using the Atomistic 3D Builder in BIOVIA Material Studio (2017). Geometry optimization was performed using the Forcite module to achieve minimized energy conformations and stable molecular configurations. The COMPASS forcefield was applied for geometry optimization, and convergence criteria were strictly observed to ensure the optimized geometries represented ground-state configurations suitable for further quantum and molecular simulations. [16].

$$\Delta E = E_L - E_H \quad (1)$$

$$IE = -E_H \quad (2)$$

$$EA = -E_L \quad (3)$$

$$\chi = \frac{1}{2}(IE + EA) \quad (4)$$

$$\eta = \frac{1}{2}(IE - EA) \quad (5)$$

$$\sigma = \frac{1}{\eta} \quad (6)$$

2.2 Quantum chemical computations

Quantum calculations were carried out using the Dmol³ module based on DFT, employing the Becke–three–Lee–Yang–Parr (B3LYP) functional and double numeric plus polarization (DNP) basis set. The calculations provided frontier orbital energies (E_H and E_L), energy gap (ΔE), ionization energy (IE), electron affinity (EA), electronegativity (χ), global hardness (η), and global softness (σ), which are essential descriptors of chemical reactivity and adsorption potential. These properties were computed using the following equations [17]:

2.3 Fukui indices and Mulliken atomic charges

Fukui functions were calculated to determine reactive centers prone to electrophilic or nucleophilic attacks. The values f^+ and f^- describe regions of electron donation and acceptance, respectively. Mulliken population analysis was used to estimate atomic charges and localized electron-rich and electron-deficient centers [18]. These analyses were performed on the optimized molecular geometries and were used to identify probable adsorption sites.

2.4 Molecular dynamics simulation

Adsorption simulations were conducted on Fe(110) surface using the Adsorption Locator and Forcite modules within BIOVIA Material Studio. The Fe metal was cleaved along the (1:1:0) plane and expanded into a 5×5 supercell to ensure a representative model of the steel surface. A vacuum space of 15 Å was introduced along the z-direction to prevent interaction between periodic images. Each molecule was initially placed 5 Å above the surface, and dynamic simulations were carried out under COMPASS forcefield [18] to obtain stable adsorption configurations. The simulations were run under the canonical ensemble (NVT) at 298 K, with temperature controlled via the Nosé–Hoover thermostat. The time step was set to 1.0 fs, and the total simulation time was 100 ps. Adsorption behavior was analyzed by monitoring the energy and configuration of the inhibitor during the trajectory. The most stable structure was selected for energy and orientation analysis.

Energy parameters including adsorption energy (E_{ads}), deformation energy (E_{def}), and rigid adsorption energy (E_{ra}) were extracted to evaluate the nature and strength of molecule-surface interactions.

3. Results and discussion

3.1 Geometry optimization

The optimized geometry of the studied compounds are shown in Figure 2. All the molecules converged to planar geometries with minimized energy configurations. Convergence plots and energy minima (depicted in Figure 3.) confirm the thermodynamic stability of each optimized structure. The pteridine backbone and its derivatives show planar configuration which is essential for facilitation of favourable adsorptive interactions with the flat Fe(110) surface. Molecules with planar geometry typically show enhanced corrosion inhibition due to greater surface coverage, allowing more effective barrier formation [18].

3.2 Frontier molecular orbitals and donor-acceptor character

The frontier molecular orbitals, namely, the HOMO (Highest Occupied Molecular Orbital) and the LUMO (Lowest Unoccupied Molecular Orbital), are central to understanding the interaction between inhibitor molecules and metal surfaces. The energy gap (ΔE) reflects the overall chemical reactivity and stability of the molecule. Uusally, smaller ΔE indicates higher reactivity and better electron donation/acceptance capability, both of which are beneficial for surface adsorption and corrosion inhibition [19]. As presented in Table 1, all the studied pteridine-based compounds exhibit negative HOMO and LUMO energies, indicating that they

are thermodynamically stable molecules and capable of participating in charge-transfer interactions with the Fe(110) surface [20].

Among the five compounds, leucopterin (E_H = -0.24674 Ha) and lumazine (E_H = -0.25745 Ha) possess the lowest HOMO energies, implying relatively poor electron-donating capabilities compared to isoxanthopterin (E_H = -0.20774 Ha) and xanthopterin (E_H = -0.20886 Ha). A high-lying HOMO (with less negative E_H) implies greater ease in donating electrons to the vacant d-orbitals of iron during adsorption [16]. The increased HOMO level in isoxanthopterin and xanthopterin may be attributed to the presence of electron-donating oxygen and nitrogen groups in conjugation with the pteridine core, particularly hydroxyl and carbonyl moieties that promote electron delocalization over the heterocyclic ring. The substitution pattern in these molecules, such as keto-enol tautomers and adjacent amino groups, could enhance orbital overlap and frontier orbital density, especially around reactive centers.

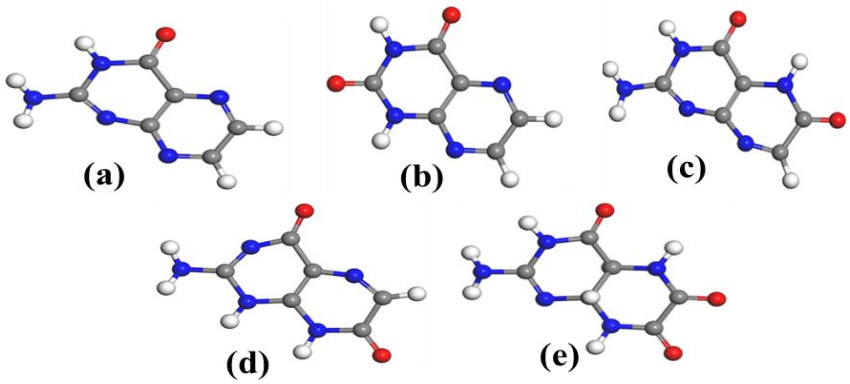

Figure 2. Optimized geometry of (a) pterin (b) lumazine (c) xanthopterin (d) isoxanthopterin and (e) leucopterin. [C = grey; N = blue; O = red; H = white].

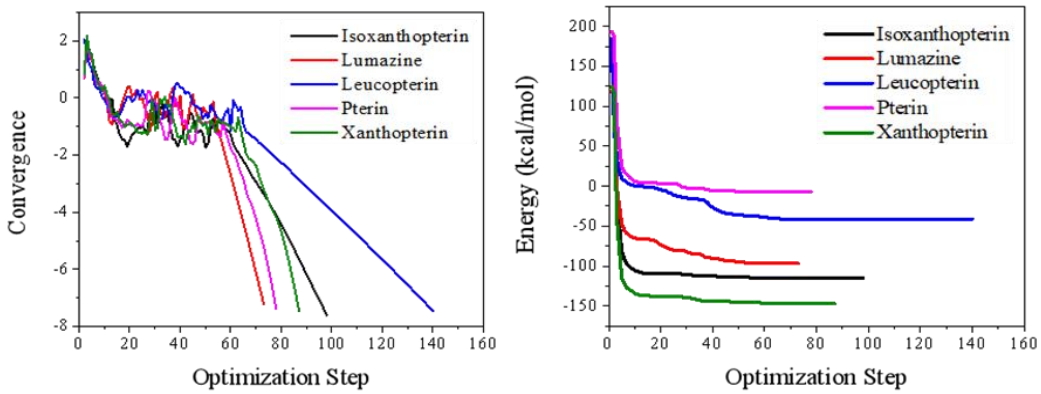

Figure 3. Convergence and energy minima plots from geometry optimization of the Pteridine-based compounds.

The E_L values show a similar trend. Leucopterin exhibited the highest (least negative) E_L of -0.04824 Ha, and this indicates that it is less capable of accepting electrons via back-donation from Fe surface orbitals. In contrast, lumazine (E_L = -0.08557 Ha) and xanthopterin (E_L = -0.08271 Ha) had lower LUMO energies, indicating stronger acceptor ability. This enhances the likelihood of forming back-donation coordinate bonds, especially involving the 3d electrons of Fe and LUMO-centered regions on the molecule. Overall, the results demonstrate that xanthopterin possesses a balanced combination of high E_H (good donor) and low E_L (good acceptor) characteristics, which may account for its relatively high adsorption energy (discussed later) and strong surface affinity.

3.3 Energy gap

The ΔE is a direct predictor of molecular reactivity. It has been documented that smaller ΔE values indicate increased ease of charge transfer, enhanced reactivity, and stronger interaction with the metal surface [21]. As shown in Table 1, it can be implied that xanthopterin with ΔE = 0.12615 Ha would be the most most reactive, followed by isoxanthopterin (ΔE = 0.14441 Ha), pterin (ΔE = 0.14955 Ha), lumazine (ΔE = 0.17188 Ha) while leucopterin (ΔE = 0.19850 Ha) would be the least reactive.

This trend correlates with the type and number of electron-donating or electron-withdrawing substituents on the pteridine backbone. Xanthopterin and isoxanthopterin both have multiple hydroxyl and carbonyl groups, capable of providing resonance stabilization and better orbital overlap. These features enhance both nucleophilicity and electrophilicity, making the compounds well-suited for both forward and backward electron flow at the metal interface.

3.4 Ionization energy and electron affinity

Lower ionization energy (*IE*) often portrays that a molecule can more readily donate electrons to the Fe surface, and can facilitate adsorption through electrostatic or donor-acceptor mechanisms. From the results, isoxanthopterin (*IE* = 0.2077 Ha) and xanthopterin (*IE* = 0.2089 Ha) show lower *IE* values than leucopterin (0.2467 Ha) and lumazine (0.2575 Ha). Electron affinity (*EA*), on the other hand, signifies a the ability of the molecule to accept electrons from the metal. A higher *EA* is desirable in chemisorption scenarios involving back-donation from the metal to the antibonding orbitals of the inhibitor molecule. Again, xanthopterin and lumazine displayed higher *EA* values compared to the others, further supporting their roles as dual-functioning electron acceptors and donors.

3.5 Global hardness and softness

Global hardness (η) describes the resistance of a molecule to charge transfer, while softness (σ = 1/η) reflects the polarizability and readiness to undergo deformation during bonding [22]. The results revealed descending trend in η values and aligns inversely with softness. Thus, xanthopterin (η = 0.0631 Ha, σ = 15.85) would be the most soft/reactive of the five, followed by isoxanthopterin (η = 0.0722 Ha, σ = 13.85), then pterin (η = 0.0748 Ha, σ = 13.37), lumazine (η = 0.0859 Ha, σ = 11.64) whereas leucopterin with η = 0.0993 Ha and σ = 10.08 would be the most hard/least reactive molecule. Xanthopterin, with the lowest global hardness and highest softness, would be more chemically flexible and capable of adapting its electron density for bonding interactions. This molecular trait is advantageous for chemisorptive interactions with Fe surface, where electronic rearrangement upon bonding is crucial [23].

3.6 Electronegativity

Electronegativity is a measure of the tendency of a molecule to attract shared electrons. On the Pauling scale, molecules with lower electronegativity values (relative to that of iron (1.83) tend to be better electron donors and form stronger adsorptive bonds [24, 25]. In this study, isoxanthopterin (χ = 0.1355) and pterin (χ = 0.1409) exhibited the lowest electronegativity values, and would probably exhibit the stronger Fe–inhibitor interaction due to greater charge disparity.

3.7 Structure–property relationships

Although the fused pteridine ring system is common to all the five studied compounds, they differ in their functional groups and some attached atoms, which will directly influence their orbital energies and adsorption characteristics. For instance, isoxanthopterin and xanthopterin contain conjugated carbonyl and hydroxyl groups, which promote electron delocalization across the ring, reduce Δ*E*, and increase softness. In leucopterin, substitution with additional amine/amide groups creates localized lone pairs but limits π-conjugation, resulting in higher hardness and reduced reactivity. Lumazine and pterin possess a balance of carbonyl and amino functionalities, but lack the multiple resonance pathways seen in isoxanthopterin or xanthopterin. A comparative analysis of the molecules reveals that the electron-rich heteroatoms (O, N) and extended π-systems of isoxanthopterin and xanthopterin could enhance their reactivity and adsorption potential, also pointing to possibility of high performance in corrosion inhibition.

Table 1. Quantum chemical descriptors of studied pteridine-based compounds.

Parameters (Ha)	Isoxanthopterin	Lumazine	Leucopterin	Pterin	Xanthopterin
E_{HOMO}	**-0.20774**	-0.25745	-0.24674	-0.21570	-0.20886
E_{LUMO}	-0.06333	-0.08557	**-0.04824**	-0.06615	-0.08271
ΔE	0.14441	0.17188	**0.1985**	0.14955	0.12615
IE	0.20774	**0.25745**	0.24674	0.21570	0.20886
EA	0.06333	**0.08557**	0.04824	0.06615	0.08271
χ	0.135535	**0.17151**	0.14749	0.140925	0.145785
η	0.072185	0.08594	**0.09925**	0.074775	0.063075
σ	13.85329	11.6360	10.0755	13.3734	**15.8541**
BE	-42.4039294	-39.1904588	-47.0898610	**-38.0371353**	-42.3987604

3.8 Frontier molecular orbitals topology

The spatial distribution of the HOMO and LUMO orbitals is very vital in understanding how each pteridine-based compound would interact with the Fe(110) surface. From the orbital plots shown in Figure 4 and 5, all the molecules exhibited π-electron density broadly delocalized across the conjugated pteridine ring system, a characteristic that supports wide and stable surface contact through planar adsorption. This planar topology is beneficial because it maximizes surface coverage and facilitates stronger molecule–surface interactions.

The HOMO and LUMO isosurfaces at an isovalue of 0.02 a.u., with blue and yellow lobes representing opposite orbital phases. Isoxanthopterin and xanthopterin, in particular, showed dense HOMO lobes localized over the nitrogen at position N7 and the adjacent carbonyl oxygen atoms (O12 and O13). This electronic configuration suggests a strong ability to donate electron density to the partially filled d-orbitals of the iron atoms, forming stable coordination bonds. Lumazine and pterin, while similarly planar, showed LUMO density concentrated around the C8=C9 to N10 segment. This electronic pattern would enhance their abilities to accept electron density via back-donation from the Fe surface, though perhaps not as effectively as in isoxanthopterin or xanthopterin. Leucopterin presented a different case as its orbital densities are less conjugated and more localized, likely due to the presence of bulky amide and amino groups that disrupt extended delocalization. As a result, the HOMO and LUMO orbitals in leucopterin are less efficiently positioned for surface interactions, which may portray a weaker overall adsorption behavior.

3.9 Fukui functions and active adsorption site analysis

Insights into the potential adsorption sites on the studied molecules were obtained by analysis of the Fukui indices and Mulliken charges displayed in Table 2 and 3 respectively. In all molecules, the N7 atom, which is the ring nitrogen situated between two conjugated systems, emerged as a consistent nucleophilic center (Figure 6). This is an ideal site for electron donation to the Fe surface, especially given its lone pair orientation and partial negative charge (typically around −0.28 to −0.31 e). The highly electrophilic oxygen atoms, specifically O12 and O13, associated with carbonyl groups also complemented the N7 atom in this regard. These atoms frequently showed the highest Fukui electrophilic indices and bore substantial negative charges (−0.41 to −0.46 e), making them suitable for accepting electron density via back-donation from the iron surface. The spatial proximity of N7 to these carbonyl groups facilitates a bidentate binding arrangement where both N and O atoms could interact simultaneously with the metal surface, forming a quasi-chelating complex.

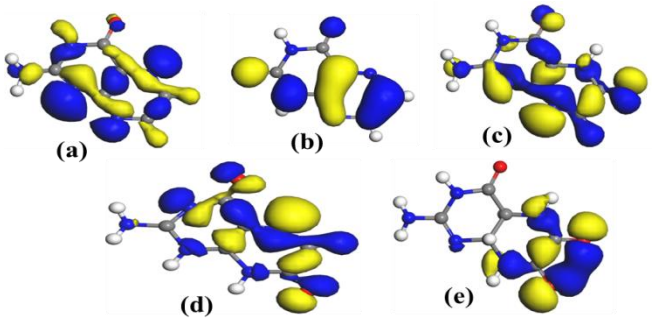

Figure 4. HOMO topology of (a) pterin (b) lumazine (c) xanthopterin (d) isoxanthopterin and (e) leucopterin. [Atoms: C = grey; N = blue; O = red; H = white. Lobes: Blue = positive phase molecular orbital; Yellow = negative phase molecular orbital].

In isoxanthopterin and xanthopterin, this N–C=C–O system is fully conjugated, and this could enable synergistic charge flow that stabilizes the adsorbed state. However, in Leucopterin, the amino and amide groups near the reactive centers disrupt this conjugation and shift the electronic density distribution. This results in a less polarized molecule with weaker interaction capability, both in donation and acceptance, which could convey inferior adsorptive and corrosion inhibition performance on the molecule.

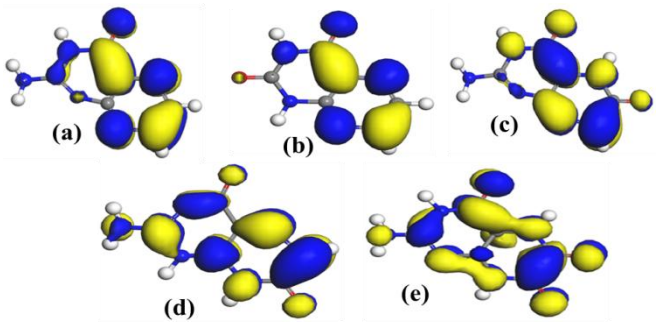

Figure 5. LUMO topology of (a) pterin (b) lumazine (c) xanthopterin (d) isoxanthopterin and (e) leucopterin. [Atoms: C = grey; N = blue; O = red; H = white. Lobes: Blue = positive phase molecular orbital; Yellow = negative phase molecular orbital].

3.10 Molecular dynamics simulation and adsorption behaviour

The final adsorption geometries and energetics, derived from molecular dynamics simulations, paint a clear comparative picture. Isoxanthopterin exhibited the strongest adsorption to the Fe(110) surface, with a highly negative adsorption energy (Table 4) indicative of favourable adsorptive interaction. Its bidentate configuration, which could anchor through N7 and a carbonyl oxygen, enhances the ability of the molecule to sit nearly flat against the metal surface (Figure 8), ensuring maximum orbital overlap and strong coordination bonds.

Table 2(a). Fukui Indices for nucleophilic attack.

Isoxanthopterin	Leucopterin	Lumazine	Pterin	Xanthopterin
C (1) 0.069	C (1) 0.048	C (1) 0.009	C (1) 0.042	C (1) 0.038
N (2) -0.000	N (2) 0.056	N (2) 0.011	N (2) 0.016	N (2) 0.015
C (3) 0.090	C (3) -0.019	C (3) 0.026	C (3) 0.026	C (3) 0.051
C (4) 0.003	C (4) -0.025	C (4) 0.070	C (4) 0.046	C (4) 0.072
C (5) 0.037	C (5) 0.092	C (5) 0.060	C (5) 0.073	C (5) 0.057
N (6) 0.042	N (6) 0.005	N (6) 0.016	N (6) 0.011	N (6) 0.026
N (7) 0.084	N (7) 0.011	**N (7) 0.132**	**N (7) 0.131**	N (7) 0.041
C (8) 0.138	C (8) 0.066	C (8) 0.011	C (8) 0.018	C (8) 0.004
C (9) 0.020	C (9) 0.064	C (9) 0.112	C (9) 0.092	**C (9) 0.159**
N (10) 0.034	N (10) 0.014	N (10) 0.101	N (10) 0.114	N (10) 0.064
N (11) 0.044	**O (11) 0.112**	O (11) 0.111	N (11) 0.038	N (11) 0.035
O (12) 0.102	**O (12) 0.112**	O (12) 0.081	O (12) 0.113	O (12) 0.096
O (13) 0.090	O (13) 0.110	H (13) 0.042	H (13) 0.048	O (13) 0.103
H (14) 0.044	N (14) 0.036	H (14) 0.044	H (14) 0.082	H (14) 0.049
H (15) 0.084	H (15) 0.051	H (15) 0.083	H (15) 0.089	H (15) 0.046
H (16) 0.050	H (16) 0.079	H (16) 0.091	H (16) 0.031	H (16) 0.086
H (17) 0.033	H (17) 0.043		H (17) 0.030	H (17) 0.029
H (18) 0.037	H (18) 0.041			H (18) 0.029
	H (19) 0.045			
	H (20) 0.030			
	H (21) 0.030			

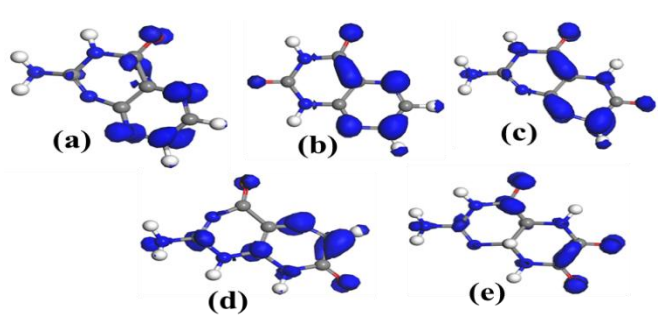

Figure 6. Fukui field (nucleophilic) of (a) pterin (b) lumazine (c) xanthopterin (d) isoxanthopterin and (e) leucopterin. [C = grey; N = blue; O = red; H = white].

The xanthopterin followed closely, showing similar geometry and surface interaction strength. The orientation of its functional groups enabled effective interaction with both the Fe atoms and surface-bound water molecules, likely through a combination of electrostatic and coordinate bonding. Pterin and lumazine molecules displayed moderate adsorption strength. Their binding involved mainly the nitrogen center (N7) and planar π-system interaction with the iron surface, the so-called monodentate-plus-π configurations. These interactions would still be stable but less robust compared to the dual anchoring observed in isoxanthopterin. Leucopterin molecule deviated sharply from the rest. Its bulky side groups may have likely distorted its ability to lie flat on the surface, and its preferred mode of interaction would likely be via hydrogen bonding rather than strong coordination. This possibly resulted in longer adsorption distances, weaker binding energies, and less stable adsorbate configurations. The electronic and steric features of leucopterin may not have favoured efficient surface adhesion.

Table 2(b). Fukui indices for electrophilic attack.

Isoxanthopterin	Leucopterin	Lumazine	Pterin	Xanthopterin
C (1) 0.037	C (1) 0.015	C (1) 0.020	C (1) 0.065	C (1) 0.046
N (2) 0.009	N (2) 0.002	N (2) 0.102	**N (2) 0.152**	N (2) 0.043
C (3) 0.051	C (3) -0.021	C (3) 0.031	C (3) 0.044	C (3) 0.055
C (4) 0.011	C (4) -0.019	C (4) 0.084	C (4) 0.040	C (4) 0.040
C (5) 0.036	C (5) -0.001	C (5) 0.015	C (5) 0.021	C (5) 0.028
N (6) 0.045	N (6) 0.010	N (6) 0.013	N (6) 0.013	N (6) 0.018
N (7) 0.173	N (7) 0.046	N (7) 0.047	N (7) 0.095	N (7) 0.038
C (8) 0.064	C (8) 0.058	C (8) 0.083	C (8) 0.039	C (8) 0.020
C (9) 0.030	C (9) 0.064	C (9) 0.040	C (9) 0.029	C (9) 0.069
N (10) 0.015	N (10) 0.061	N (10) 0.061	N (10) 0.072	N (10) 0.105
N (11) 0.036	O (11) 0.041	O (11) 0.096	N (11) 0.046	N (11) 0.052
O (12) 0.139	O (12) 0.206	**O (12) 0.149**	O (12) 0.083	**O (12) 0.147**
O (13) 0.098	**O (13) 0.233**	H (13) 0.056	H (13) 0.060	O (13) 0.092
H (14) 0.049	N (14) 0.025	H (14) 0.043	H (14) 0.080	H (14) 0.045
H (15) 0.098	H (15) 0.050	H (15) 0.084	H (15) 0.080	H (15) 0.047
H (16) 0.050	H (16) 0.045	H (16) 0.076	H (16) 0.037	H (16) 0.088
H (17) 0.028	H (17) 0.030		H (17) 0.045	H (17) 0.031
H (18) 0.029	H (18) 0.056			H (18) 0.035
	H (19) 0.061			
	H (20) 0.017			
	H (21) 0.022			

Overall, the trend in adsorption strength and surface orientation mirrors the earlier quantum reactivity findings. The more conjugated and electron-soft molecules, especially those with dual reactive centers, formed tighter, more stable binding interactions with the Fe(110) surface. Molecules with disrupted planarity or localized electronic density, such as leucopterin, underperformed due to limited orbital overlap and weaker charge-transfer capability. The compounds likely to be highly efficient as corrosion inhibitors shared three traits. First is planarity, which ensures broad contact with the Fe(110) terrace. The second is presence of dual reactive centers (nucleophilic nitrogen and electrophilic oxygen) that allow both electron donation and acceptance. The third trait is the presence of conjugation across the pteridine moeity, which lowers the HOMO-LUMO gap and facilitates dynamic electron flow. Isoxanthopterin and xanthopterin molecules exhibited all these three traits and could be considered as the most promising corrosion inhibitors in the series. Pterin and lumazine, though chemically suitable, lack the optimal geometry or electron distribution for maximal inhibition, but could exhibit average to good corrosion inhibition performance. Leucopterin, encumbered by electronic isolation and steric hindrance, was the least effective and my not be a very promising inhibitor.

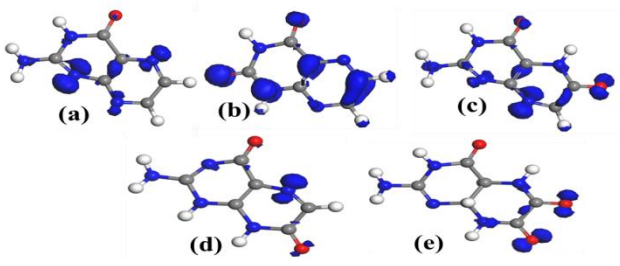

Figure 7. Fukui field (electrophilic) of (a) pterin (b) lumazine (c) xanthopterin (d) isoxanthopterin and (e) leucopterin.

3.11 Nature of adsorption and structural influence

The computed adsorption energies were all below –1.0 eV (-0.0367 Ha) and the interaction distances calculated between heteroatoms (N, O) and the Fe(110) surface were less than 2.5 Å. These values portray that the molecules would adsorb primarily through chemisorption rather than weak physisorption. This would imply significant orbital overlap and charge transfer, consistent with the strong adsorption behavior observed. Structural factors such as molecular planarity and steric hindrance play key roles in modulating adsorption strength. Planar derivatives (e.g., lumazine, pterin) adopt near-parallel orientations on the surface, as confirmed by small tilt angles (;ess than 15°) and minimal centroid-to-surface distances (about 2.0 Å). This favours strong surface contact. In contrast, bulkier or twisted structures exhibit reduced planarity, larger tilt angles (more than 25°), and diminished interaction, reflected in slightly lower adsorption energies.

Table 3. Mulliken atomic charges.

Isoxanthopterin	Leucopterin	Lumazine	Pterin	Xanthopterin
C (1) 0.514	C (1) 0.535	**C (1) 0.657**	C (1) 0.500	C (1) 0.483
N (2) -0.479	N (2) -0.435	N (2) -0.365	N (2) -0.347	N (2) -0.332
C (3) 0.456	C (3) 0.175	C (3) 0.401	C (3) 0.381	C (3) 0.403
C (4) 0.082	C (4) -0.051	C (4) 0.057	C (4) 0.060	C (4) 0.112
C (5) 0.447	**C (5) 0.573**	C (5) 0.512	**C (5) 0.514**	**C (5) 0.512**
N (6) -0.342	N (6) -0.439	N (6) -0.421	**N (6) -0.470**	**N (6) -0.472**
N (7) -0.216	N (7) -0.411	N (7) -0.286	N (7) -0.296	N (7) -0.454
C (8) -0.003	C (8) 0.473	C (8) 0.066	C (8) 0.065	C (8) 0.493
C (9) 0.493	C (9) 0.463	C (9) 0.088	C (9) 0.083	C (9) 0.019
N (10) -0.467	N (10) -0.377	N (10) -0.355	N (10) -0.335	N (10) -0.272
N (11) -0.406	**O (11) -0.452**	O (11) -0.433	N (11) -0.411	N (11) -0.411
O (12) -0.463	O (12) -0.417	**O (12) -0.483**	O (12) -0.422	O (12) -0.463
O (13) -0.436	O (13) -0.420	H (13) 0.233	H (13) 0.204	O (13) -0.463
H (14) 0.193	N (14) -0.406	H (14) 0.238	H (14) 0.087	H (14) 0.206
H (15) 0.106	H (15) 0.096	H (15) 0.096	H (15) 0.087	H (15) 0.235
H (16) 0.211	H (16) 0.133	H (16) 0.096	H (16) 0.206	H (16) 0.106
H (17) 0.190	H (17) 0.219		H (17) 0.193	H (17) 0.207
H (18) 0.218	H (18) 0.230			H (18) 0.191
	H (19) 0.213			
	H (20) 0.209			
	H (21) 0.187			

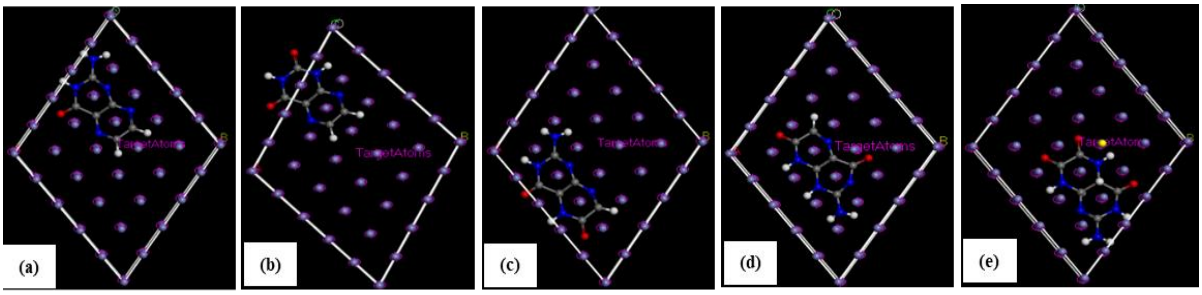

Figure 8. Front view of the adsorption of (a) pterin (b) lumazine (c) xanthopterin (d) isoxanthopterin and (e) leucopterin on Fe(110) surface determined by MDS.

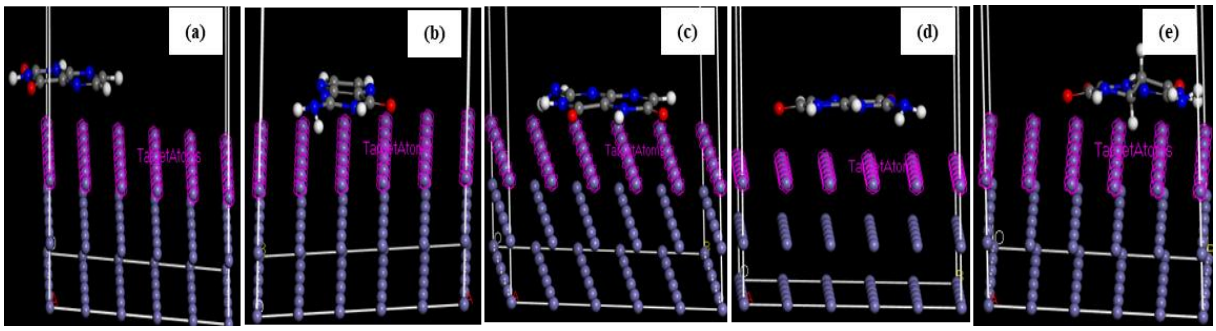

Figure 9. Side view of the adsorption of (a) pterin (b) lumazine (c) xanthopterin (d) isoxanthopterin and (e) leucopterin on Fe(110) surface determined by molecular dynamics simulation.

Table 4. Adsorption related energies of the pteridine-based compounds obtained by molecular dynamics simulation.

Energy (Ha)	Isoxanthopterin	Lumazine	Leucopterin	Pterin	Xanthopterin
E_{total}	-208.8268	-182.6136	-143.1899	-90.8862	-242.1376
E_{ads}	-93.8514	-86.1138	-101.8881	-83.5842	-95.3845
E_{ra}	-94.1422	-86.4708	-103.5770	-83.9460	-95.7044
E_{def}	0.2908	0.3570	1.6889	0.3618	0.31995

3.12 Correlation between electronic descriptors and adsorption energy

In order to further investigate the structure–activity relationship of the studied pteridine derivatives, the correlation between their adsorption energies on the Fe(110) surface and selected global electronic descriptors, namely, global softness (S) and the HOMO–LUMO energy gap (ΔE), was analysed. The resulting plots are shown in Figure 9. As indicated by the Pearson correlation coefficients (r), the relationship between adsorption energy and these descriptors is relatively weak. Specifically, the correlation between adsorption energy and global softness yielded r-value of 0.1984 which portrays only a marginal positive association (Figure 9a). The correlation between adsorption energy and HOMO-LUMO energy gap produced r-value of –0.2839, also indicating a weak inverse relationship (Figure 9b). It can be inferred from these findings that, while electronic descriptors such as ΔE and softness influence reactivity to some degree, they do not solely govern the adsorption behavior of these molecules on the Fe(110) surface. The relatively low correlation values imply that other factors, which may include molecular orientation, adsorption site preferences, intermolecular interactions and surface charge effects, likely play significant roles in determining adsorption strength [26].

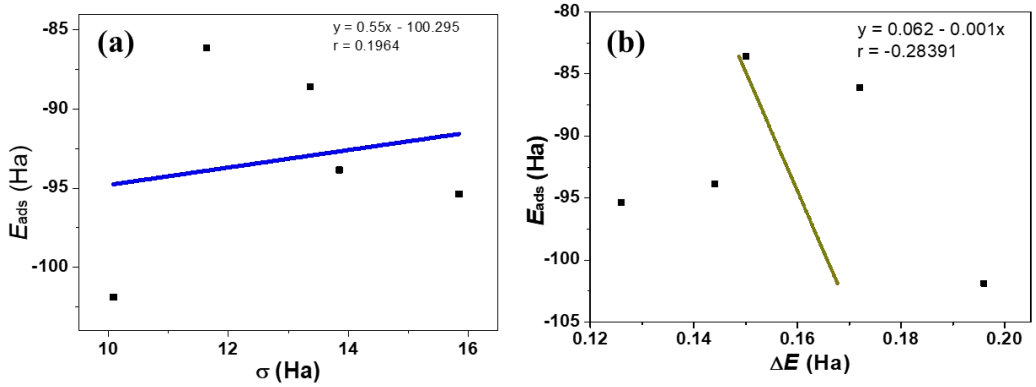

Figure 9. Scatter diagram showing correlation between adsorption energy of the studid compounds and (a) global softness (b) HOMO-LUMO energy gap.

3.13 Summary of findings

This study applied density functional theory (DFT) and molecular dynamics (MD) simulations to investigate the adsorption behavior and corrosion inhibition potential of five pteridine-based compounds, namely, isoxanthopterin, xanthopterin, lumazine, pterin and leucopterin, on Fe(110) surface. Through a combination of quantum chemical descriptors, frontier molecular orbital analysis, Fukui function assessment, and dynamic adsorption modeling, the relationship between molecular structure and inhibitory performance was systematically elucidated. Among the studied compounds, isoxanthopterin and xanthopterin demonstrated the most favorable electronic and adsorption characteristics. Their relatively high-lying HOMO levels, low HOMO-LUMO energy gaps, and high global softness revealed a strong tendency toward chemical reactivity and surface affinity. These features were supported by rich electron-donating nitrogen centers (N7) and electron-accepting carbonyl groups (O12/O13) strategically positioned within a conjugated, planar backbone, an arrangement that facilitates dual-site adsorption and optimal Fe-surface interaction.

Leucopterin, which lacked extensive π-conjugation and bore bulky, electronically isolating side chains, displayed a significantly reduced adsorption energy and weaker molecular surface interactions. Pterin and Lumazine, while electronically active, showed intermediate performance due to limited orbital symmetry and less effective charge transfer configurations. This work underscores the critical role of molecular planarity, conjugation, and functional group positioning in defining corrosion inhibition performance. It also demonstrates the power of computational modelling not only as a predictive tool but as a cost-effective complement to experimental approaches in corrosion science. From a practical perspective, isoxanthopterin and xanthopterin could be promising lead structures for the design of green, efficient, and structurally tunable corrosion inhibitors for steel protection.

3.14 Limitations and future work

While the present study provides valuable insights into the adsorption behaviour and inhibition potential of some pteridine-

based compounds using DFT and MD simulations, certain limitations must be acknowledged. First, the simulations were performed in vacuum, without accounting for solvation effects, which can influence adsorption energies and molecular orientation through dielectric screening and hydrogen bonding interactions. Future studies could incorporate implicit or explicit solvent models to better replicate the aqueous or acidic environments typical of corrosion systems. Second, temperature effects were only partially addressed through MD simulations at room temperature. Incorporating annealing protocols or temperature-dependent modeling could yield a more dynamic picture of adsorption stability under real-world corrosion conditions.

Thirdly, while our results provide predictive insights, experimental validation, with techniques such as electrochemical measurements, surface characterization (e.g., SEM, XPS), and inhibitor performance tests, will be essential to confirm the theoretical trends and translate these findings into practical corrosion inhibition applications. Lastly, hile the present analysis was based on gas-phase electronic descriptors, further insight into the metal-inhibitor interaction could be obtained through post-adsorption electron density analyses, such as electron localization function (ELF) and charge density difference mapping. These could be considered in future studies to directly probe the nature and extent of electronic charge redistribution upon adsorption.

4. Conclusion

Density functional theory (B3LYP/DNP) and molecular-dynamics simulations were combined to elucidate the interaction of five pteridine derivatives, namely, isoxanthopterin, xanthopterin, lumazine, pterin and leucopterin with the Fe(110) surface. Geometry optimisations returned highly planar backbones that favour extensive surface coverage. Isoxanthopterin and xanthopterin exhibited the most desirable electronic traits: high-lying HOMO levels (≈ –0.21 Ha), the lowest HOMO–LUMO gaps (0.13–0.14 Ha) and the greatest global softness, signalling facile charge exchange. Fukui and Mulliken analyses pinpointed N7 (nucleophilic) and the adjacent carbonyl oxygens (electrophilic) as dual reactive centres, enabling simultaneous σ-donation and π-back-donation with iron. Molecular dynamic simulations confirmed bidentate N/O anchoring at separations of ≈ 2.1 Å and yielded the most exergonic adsorption energies (–47 and –42 kcal mol^{-1} for isoxanthopterin and xanthopterin, respectively). Lumazine and pterin adsorbed in a weaker monodentate-plus-π fashion, while bulky, poorly conjugated leucopterin relied mainly on hydrogen bonding, giving the least stable film. The combined results reveal that planarity, extended π-conjugation and strategically placed N–C=C–O motifs are decisive for high inhibition efficiency. Isoxanthopterin and xanthopterin were therefore considered the most promising lead scaffolds for environmentally benign steel protectants. The structure–property insights offered in this study provide a clear roadmap for further molecular optimisation and experimental validation.

Acknowledgments

The authors appreciate the support of Tertiary Education Trust Fund (TETFund) of Federal Republic of Nigeria, through the TETFund Centre of Excellence in Computational Intelligence Research as well as the Management of the University of Uyo, Uyo, Nigeria.

References

[1] Holla B. R., Mahesh R., Manjunath H. R. and Anjanapura V. R., Plant extracts as green corrosion inhibitors for different kinds of steel: a review. *Heliyon,* **10** (2024), e33748.

[2] Shwetha K. M., Praveen B. M. and Devendra B. K., A review on corrosion inhibitors: types, mechanisms, electrochemical analysis, corrosion rate and efficiency of corrosion inhibitors on mild steel in an acidic environment. *Results Surf. Interfaces,* **16** (2024), 100258.

[3] Ahmed M. A., Amin S. and Mohamed A. A., Current and emerging trends of inorganic, organic and eco-friendly corrosion inhibitors. *RSC Adv.,* **14** (43) (2024), 31877–31920.

[4] Al-Amiery A. A., Isahak W. N. R. W. and Al-Azzawi W. K., Corrosion inhibitors: natural and synthetic organic inhibitors. *Lubricants,* **11** (4) (2023), 174.

[5] Răuță D. I., Matei E. and Avramescu S. M., Recent development of corrosion inhibitors: types, mechanisms, electrochemical behavior, efficiency, and environmental impact. *Technol.,* **13** (3) (2025), 103.

[6] Shwetha K. M., Praveen B. M. and Devendra B. K., A review on corrosion inhibitors: types, mechanisms, electrochemical analysis, corrosion rate and efficiency of corrosion inhibitors on mild steel in an acidic environment. *Results Surf. Interfaces,* **16** (2024), 100258.

[7] Wang J., An L., Wang J., Gu J., Sun J. and Wang X., Frontiers and advances in N-heterocycle compounds as corrosion inhibitors in acid medium: recent advances. *Adv. Colloid Interface Sci.,* **321** (2023), 103031.

[8] Verma C., Rhee K. Y., Quraishi M. A. and Ebenso E. E., Pyridine based N-heterocyclic compounds as aqueous phase corrosion inhibitors: a review. *J. Taiwan Inst. Chem. Eng.,* **117** (2020), 265–277.

[9] Kadhim A., Betti N., Al-Bahrani H. A., Al-Ghezi M. K. S., Gaaz T., Kadhum A. H. and Alamiery A., A mini review on corrosion, inhibitors and mechanism types of mild steel inhibition in an acidic environment. *Int. J. Corros. Scale Inhib.,* **10** (3) (2021), 861–884.

[10] Nyangiwe N. N., Applications of density functional theory and machine learning in nanomaterials: a review. *Next Mater.,* **8** (2025), 100683.

[11] Salahshoori I., Mahdavi S., Moradi Z., Otadi M., Kazemabadi F. Z., Nobre M. A., Khonakdar H. A., Baghban A., Wang Q. and Mohammadi A. H., Advancements in molecular simulation for understanding pharmaceutical pollutant adsorption: a state-of-the-art review. *J. Mol. Liq.,* **410** (2024), 125513.

[12] Verma D. K., Aslam R., Aslam J., Quraishi M. A., Ebenso E. E. and Verma C., Computational modeling: theoretical predictive tools for designing of potential organic corrosion inhibitors. *J. Mol. Struct.,* **1236** (2021), 130294.

[13] Ituen E., Mkpenie V., Moses E. and Obot I., Electrochemical kinetics, molecular dynamics, adsorption and anticorrosion behavior of melatonin biomolecule on steel surface in acidic medium. *Bioelectrochemistry,* **129** (2019), 42–53.

[14] El-Kalyoubi S. A., Gomaa H. A., Abdelhafez E. M., Ramadan M., Agili F. and Youssif B. G., Design, synthesis, and anti-proliferative action of purine/pteridine-based

derivatives as dual inhibitors of EGFR and BRAFV600E. *Pharmaceuticals,* **16** (5) (2023), 716.

[15] Schormann N., Senkovich O., Ananthan S. and Chattopadhyay D., Docking and biological activity of pteridine analogs: search for inhibitors of pteridine reductase enzymes from *Trypanosoma cruzi. J. Mol. Struct. THEOCHEM,* **635** (1–3) (2003), 37–44.

[16] Ituen E., Etuk A., Akpan G., Affangide I., Unama I., Shaibu S. and Inyang U., Inhibition of steel corrosion in oilfield acidizing environment using cashew nut shell liquid: preliminary experimental and computational studies. *J. Mater. Environ. Sci.,* **16** (8) (2025), 1426–1437.

[17] Obot I. B., Onyeachu I. B. and Kaya S., Density Functional Theory: Practical Application and Their Limitations in Corrosion Inhibition Research. *In: Corrosion Science.* Apple Academic Press, (2023), 173–198.

[18] Oyeneyin O., Akerele D., Ojo N. and Oderinlo O., Corrosion inhibitive potentials of some 2H-1-benzopyran-2-one derivatives – DFT calculations. *Biointerf. Res. Appl. Chem.,* **11** (6) (2021), 13968–13981.

[19] Saddik A. A., Sayed M., Mohammed A. A., Abdel-Hakim M. and Ahmed M., Molecular design and performance of emissive amide-containing compounds as corrosion inhibitors: synthesis, electrochemical evaluation, DFT calculations and molecular dynamics simulations. *RSC Adv.,* **15** (19) (2025), 15384–15396.

[20] El Guesmi N., Asghar B. H., Awad M. I., Al Harbi A. N., Kassem M. A. and Shaaban M. R., Novel thiazole-derived Schiff-bases as efficient corrosion inhibitors for mild steel in acidic media: synthesis, electrochemical and computational insights. *Arab. J. Chem.,* **17** (9) (2024), 105867.

[21] Fouda A. S., Abdel-Wahed H. M., Atia M. F. and El-Hossiany A., Novel porphyrin derivatives as corrosion inhibitors for stainless steel 304 in acidic environment: synthesis, electrochemical and quantum calculation studies. *Sci. Rep.,* **13** (1) (2023), 17593.

[22] Azeez Y. H., Kareem R. O., Hamad O., Omer R., Othman K., Ahmed L. and Kaygılı O., Quantum chemical calculation employed for investigation mesitylene compound. *J. Phys. Chem. Funct. Mater.,* **7** (1) (2024), 17–27.

[23] Gázquez J. L., Hardness and Softness in Density Functional Theory. *In: Sen K.D. (ed.) Chemical Hardness. Structure and Bonding,* volume 80 of *Structure and Bonding,* Springer, Berlin, Heidelberg, (1993), 1–32.

[24] Murphy L. R., Meek T. L., Allred A. L. and Allen L. C., Evaluation and test of Pauling's electronegativity scale. *J. Phys. Chem. A,* **104** (24) (2000), 5867–5871.

[25] Ituen E., Mkpenie V., Shaibu S., Yuanhua L., Inyang U., Sun S., Nelana S., Klink M. and Ayanda O., Evaluating the potential of ataluren as X80 steel corrosion inhibitor in acid wash solution: an experimental and computational intelligence approach. *J. Corros. Sci. Technol.,* **4** (3) (2025), 134–150.

[26] Kwon S., Vidic R. and Borguet E., The effect of surface chemical functional groups on the adsorption and desorption of a polar molecule, acetone, from a model carbonaceous surface, graphite. *Surf. Sci.,* **522** (1–3) (2003), 17–26.